Journal of Electronics and Electrical Engineering
https://ojs.wiserpub.com/index.php/JEEE

UNIVERSAL WISER PUBLISHER

Research Article

Arbitrary Waveform Time-Domain Responses of RLC-Network Based BP-NGD Passive Cell

Idiris Aweis Hussein[1], Sammer Christopher Moussa[2], Florent Manorosoa Tsivery Anjara[2], Leonide Tongazara[3], Jeannot Velontsoa[3,4], Habachi Bilal[5], Sébastien Lalléchère[6], Blaise Ravelo[1*]

[1] School of Electronic and Information Engineering, Nanjing University of Information Science and Technology, Nanjing 210044, China
[2] Society for Education, Research, Development & Innovation (SERDI), Antsiranana 201, Madagascar
[3] Faculty of Sciences, University of Antsiranana, Antsiranana 201, Madagascar
[4] The Antsiranana Higher Institute of Technology (IST-D), Antsiranana 201, Madagascar
[5] Laboratory of Innovative Technologies (LTI, UR 3899), University of Picardie Jules Verne (UPJV), 80000 Amiens, France
[6] French Association for Systems, Cybernetics, Cognitive and Technical Sciences (AFSCET), 92260 Fontenay-aux-Roses, France
[*] Correspondence: blaise.ravelo@yahoo.fr

Received: 27 April 2026; **Revised:** 18 June 2026; **Accepted:** 28 June 2026; **Published:** 9 July 2026

Abstract: A time-domain investigation of a bandpass negative group delay (BP-NGD) electronic circuit is proposed in this paper by utilizing a passive cell composed of single-stage parallel resistive-inductive-capacitive-network (RLC-network). The provided configuration is analytically modelled and validated through circuit-level simulation. The BP-NGD circuit design method is elaborated. The performed study is based on both the frequency- and time-domain analyses of the considered BP-NGD passive topology within the NGD frequency band. As Virtual proof-of-concept (POC), the RLC-circuit was designed to achieve an NGD of approximately -45 µs around the center frequency of $f_n = 50$ kHz. To validate the time-advance behavior, Gaussian- and arbitrary-waveform signals modulating a sinusoidal carrier at frequency f_n are injected as inputs to the Virtual POC. Time-domain results demonstrate that the NGD behavior is manifested as an advance in the signal envelope, which does not violate causality. The performed circuit analysis establishes the effectiveness of passive RLC topologies for NGD realization in the low-frequency region with potential applications in signal synchronization and phase compensation.

Keywords: negative group delay (NGD), bandpass NGD (BP-NGD), parallel RLC network, time-domain studies, signal advancement, modulated signals

1. Introduction

Despite its counterintuitive aspect, negative group delay (NGD) phenomenon enables the electronic circuit to exhibit signal with negative delay rather than a positive delay within a defined frequency band [1–3]. The NGD phenomenon causes the output envelope peak to precede the input signal, an effect formally designated as temporal advancement [1–3]. We emphasize that this phenomenon often regards as one of the most counterintuitive to Einsteinian causality yet physically valid discoveries in electromagnetic and circuit engineering. Yet unfamiliar to non-specialists, the NGD phenomenon was a groundbreaking engineering discovery, which was attributed to its initiation in wave physics by Sommerfield 1954, Brillouin 1964 [4, 5]. The NGD study in physics was established the theoretical framework of anomalous dispersion in

DOI: https://doi.org/10.37256/jeee.52202610078

wave-propagating media that can give rise to negative group velocity later NGD [6]. Early, observations of the NGD phenomenon were reported in the optical domain by [6–13] by demonstrating negative group velocity in dispersive media. However, until the 1990s, The NGD effect was not that a significant shift occurred from optical physics to electronic circuit implementation when formally identified and experimentally demonstrated NGD behavior in electronic systems. Subsequent research efforts on the NGD were then developed the theory and practice of NGD circuits on various technologies and platforms through their experimental and theoretical works [14–18]. Consequently, numerous topologies of passive and active analog circuits capable of producing NGD effect have been systematically discovered. The configuration and implementation of NGD circuits have been studied from different technological perspectives, among them are, the transmission-line-based architectures [14, 15, 18], the engineered left-handed transmission structures [16, 17, 19], the active-lumped network [20–24] and the passive lumped networks [25–31].

In contrast, bandpass (BP) type NGD circuit based on RLC circuit topologies that exhibit BP characteristics for implementation of NGD functionality can provide greater flexibility since RLC based circuits can yield selective NGD behavior at specified frequencies for applications where filtering and delaying signals are both desired [32, 33]. There has been considerable research effort on the NGD circuit with most of these works focusing on the frequency domain in which the NGD effect is characterized by using the phase and group delay (GD) responses to the steady state behavior [34–37]. While this representation of the NGD phenomenology is useful for studying the steady-state behavior of the circuits, it does not adequately characterize the transient and signal level dynamic behaviors associated with NGD circuits. Specifically, the frequency domain does not provide an explicit representation of the time advancement phenomenon that is seen in practical signals. Therefore, it is necessary to translate and validate NGD behavior in the time domain to have an adequate understanding of the circuit performance. However, the time domain approach with respect to RLC-based BP-NGD circuits is still relatively limited in comparison to low-pass NGD circuits. Therefore, this work concentrates on performing transient analysis and validation of a bandpass (BP) type network using a parallel RLC configuration.

The subsequent sections of this paper are arranged as outlined below:

• Section 2 describes the synoptic diagram of the parallel RLC BP-NGD circuit. The associated transmission function, defined as the input-to-output ratio and the definitions of the main parameters including GD, center frequency, and envelope advancement are established.

• Section 3 formalizes the design methodology of the BP-NGD network, presenting synthesis equations to calculate resistor, inductor and capacitor values from target specification as NGD center frequency.

• Section 4 presents the Virtual proof-of-concept (POC) based on the NI MULTISIM® environment frequency-domain simulation. The calculated and simulated voltage transfer functions (VTFs) are compared to verify the BP-NGD behavior.

• Section 5 presents the Virtual POC time-domain simulation analysis from NI MULTISIM® tool, employing black-box modeling from VTF to predict and validate envelope advancement. Gaussian-modulated and arbitrary-modulated input pulse is used, with envelope extraction via Hilbert transform, demonstrating good agreement between time-domain advancement.

• Section 6 provides the conclusion.

2. Fundamental operating principle and signal behavior of the BP-NGD topology

The current section presents an operational principle governing the BP-NGD function, from which the transfer function and GD expression are subsequently derived.

2.1 *Fundamental definition of BP-NGD function*

Consider a two-port network represented as a black box with an input port and an output port, as illustrated in Figure 1. The BP-NGD function is fundamentally characterized by the behavior of the VTF of the network, wherein the GD assumes a negative value within a specified passband, rather than the positive delay exhibited by classical filter systems.

Figure 1. BP-NGD two-port black box

By interpreting and translating the Laplace variable as $s = j\omega = j2\pi f$ with angular frequency ω and frequency f, the theoretical exploration of the VTF is performed the input-to-output ratio, $V_{in}(s)$ and $V_{out}(s)$, respectively. The VTF associated with the black-box BP-NGD system shown in Figure 1 is fundamentally defined as:

$$H(j\omega) = \frac{V_{out}(j\omega)}{V_{in}(j\omega)}. \tag{1}$$

The s-domain representation enables direct analysis of the circuit's frequency-dependent transmission characteristics. Therefore, the frequency-domain transmittance is defined from the VTF $H(j\omega)$ as magnitude:

$$T(\omega) = |H(j\omega)| \tag{2}$$

which becomes:

$$T(\omega) = \sqrt{Real[H(j\omega)]^2 + Imag[H(j\omega)]^2} \tag{3}$$

where $Real(.)$ and $Imag(.)$ represent the real and imaginary parts of complex number. The associated phase is:

$$\varphi(\omega) = arg\{H(j\omega)\}. \tag{4}$$

This s-domain formulation permits direction extract of the group delay (GD) characteristics:

$$\tau_g(\omega) = -\frac{\partial\varphi(\omega)}{\partial\omega}. \tag{5}$$

The GD can be described as the negative derivative of the transmission phase with respect to the angular frequency. And as for the BP-NGD circuit, exhibits negative values at the selective center frequency $\omega_{0,}$ causing output envelope time-advancement. GD analytical expressions will be analyzed in the next subsection.

2.2 *Ideal characterization of BP-NGD frequency response function*

An analysis of the bandpass-NGD circuit necessitates characterization through key frequency-domain parameters. Accordingly, the idealized magnitude and GD response depicted in Figure 2a,b, respectively, establishes fundamentally governing RLC-network based passive topology design.

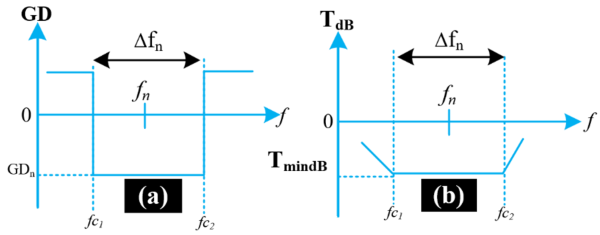

Figure 2. Ideal response of (a) GD and (b) magnitude specifications of BP-NGD function

In the context of Figure 2, the general specification can be extracted from, named as GD and magnitude response which differ fundamentally from classical filter characteristics. Therefore, BP-NGD function operates within a selective frequency band bounded by two critical frequencies, the lower cut-off frequency ω_{c1} and the upper cut-off frequency ω_{c2}, which together constitute the cutoff frequencies defining the operational bandwidth defined as:

• The BP-NGD cut-off frequencies $(\omega_{c2} > \omega_{c1})$ can be formulated as the zero-crossing points of the GD response:

$$\begin{cases} \tau_g(\omega_{c1}) = 0 \\ \tau_g(\omega_{c2}) = 0 \end{cases} \tag{6}$$

Defining the band edges where NGD begins and ends.

• The NGD center frequency f_n which can be defined as:

$$\tau_g(\omega_n) = \min\{\tau_g(\omega)\} < 0,\ \omega \in [\omega_{c1}, \omega_{c2}]\,. \tag{7}$$

The NGD bandwidth (BW) can be articulated as:

$$\Delta\omega_n = \omega_{c2} - \omega_{c1}\,. \tag{8}$$

• The network transmittance level at the frequency of maximal NGD absolute value is expressed as:

$$T(\omega_n) = |H(j\omega_n)|\,. \tag{9}$$

At the NGD center frequency ω_n, the VTF magnitude $|H(j\omega_n)|$ reaches its minimum, determining the insertion loss T_n where optimum NGD occurs.

3. Analytical framework of the passive RLC-BP-NGD circuit

This section unveils an analytical framework of passive parallel RLC BP-NGD configuration, focusing on the input-to-output ratio derivation and GD characterization to establish the temporal-advance condition in terms of the network configuration parameters.

3.1 *Topology and transfer function of the passive RLC BP-NGD network*

The proposed passive topology illustrated in Figure 3 represents the parallel RLC network-based circuit constituting the single-band BP-NGD configuration to be analytically investigated and validated through simulation in the present study.

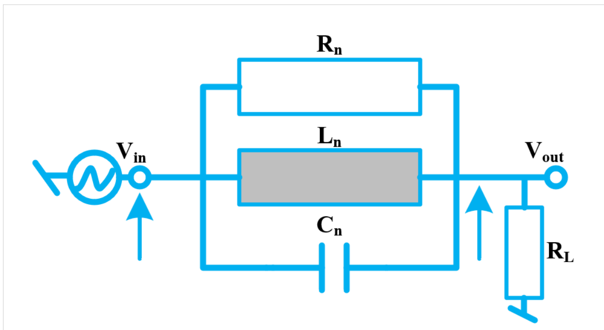

Figure 3. Passive parallel RLC BP-NGD circuit topology

The circuit comprises a parallel combination of resistor R_n, inductor, L_n, and capacitor C_n, terminated by load resistance R_L. Recalling the VTF of the passive BP-NGD network, derived by applying the voltage divider rule between the parallel RLC impedance and the load resistance R_L, the input-output magnitude is conveniently rewritten as given in (1):

$$T(\omega) = \frac{R_L\sqrt{(L_n\omega)^2 + [R_n(L_nC_n\omega^2 - 1)]^2}}{\sqrt{[(R_L+R_n)L_n\omega]^2 + [R_LR_n(L_nC_n\omega^2 - 1)]^2}}. \tag{10}$$

Nevertheless, the designated working frequency is aligned with the parallel resonance frequency of the $R_nL_nC_n$ network, expressed in angular frequency as:

$$\omega_n = \frac{1}{\sqrt{L_nC_n}}. \tag{11}$$

At this center frequency, the BP-NGD circuit attenuation factor proposed in (8) is given by:

$$T_n = \frac{R_L}{R_n + R_L}. \tag{12}$$

Additionally, τ_g at the NGD center frequency expressed in (7) becomes:

$$\tau_g(\omega_n) = \frac{-2{R_n}^2}{L_n\omega_n^2(R_L+R_n)}. \tag{13}$$

Therefore, the NGD BW defined in (8) is written as:

$$\omega_{c1} = \omega_n \sqrt{1 + 2\frac{\omega_n^2}{\omega_a^2} - \sqrt{\left(1 + 2\frac{\omega_n^2}{\omega_a^2}\right)^2 - 1}} \tag{14}$$

$$\omega_{c2} = \omega_n \sqrt{1 + 2\frac{\omega_n^2}{\omega_a^2} + \sqrt{\left(1 + 2\frac{\omega_n^2}{\omega_a^2}\right)^2 - 1}}. \tag{15}$$

Substituting the parallel-resonance condition into the attenuation-bandwidth relation yields the explicit form:

$$\omega_a = \frac{R_n}{L_n} \sqrt{\frac{\rho}{1 + \rho}} \tag{16}$$

where $\rho = R_L/R_n$ directly shows how the load-to-parallel resistance ratio controls the attenuation bandwidth. Using the theoretical framework presented above, the next section details the complete design equation for a BP-NGD circuit, allowing the values of R_n, L_n and C_n to be directly computed based on NGD specifications.

3.2 *Design equation of considered RLC-network based BP-NGD topology*

The design equations in this section allow direct synthesis of the BP-NGD circuit. Closed-form expressions are developed for calculating the values of the constituent resistors, inductors, and capacitors from target specifications target center frequency so that the circuit can be implemented practically. Knowing the attenuation T_n, R_n can be determined from equation (12) by using existing value of R_L:

$$R_n = \left(\frac{1 - T_n}{T_n}\right) R_L. \tag{17}$$

The resolution of equation $\tau_g(\omega_n) = \tau_n < 0$, enables to express the inductor value L_n, formulated as:

$$L_n = \frac{-2R_n^2}{\tau_n \omega_n^2 (R_L + R_n)}. \tag{18}$$

Recalling resonance frequency (11), this parameter is linked to the capacitance. From this relationship the capacitor value can be formulated as:

$$C_n = \frac{1}{L_n \omega_n^2}. \tag{19}$$

Thus, R_n can be arbitrarily chosen. The upcoming subsection codifies the hierarchical specification workflow, translating the preceding analytical expressions into reproducible component-synthesis protocol.

3.3 *Design methodology of BP-NGD circuit*

To demonstrate hierarchical specification workflow of the BP-NGD circuit, a stepwise flowchart is developed illustrating the hierarchical design procedure in ascending, from initial circuit selection to final NGD response validation, as depicted in Figure 4.

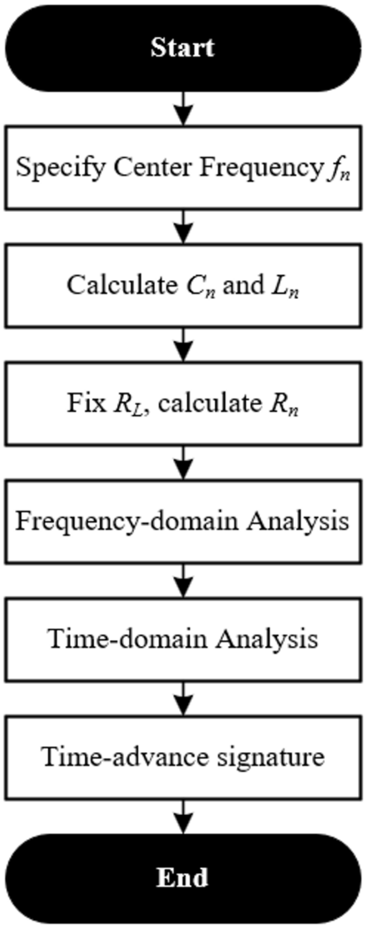

Figure 4. Flowchart illustrating the BP-NGD time-domain characterization and design methodology

The flowchart in Figure 4 outlines the BP-NGD circuit design procedure in six ascending steps, beginning with the specification of the center frequency, f_n, followed by the calculation of C_n and ln fixing R_L to determine R_n, performing frequency-domain and time-domain analyses and concluding with the verification of the time-advance signature.

4. Frequency-domain design verification of the BP-NGD Virtual POC cell

The current section presents the Virtual POC validation of the BP-NGD circuit under study in reference to the previously specified design criteria. The AC simulation response, as analytically calculated using MATLAB® is compared to simulation results obtained using NI MULTISM® to show that this topology operates as expected to produce NGD in the defined working frequency band.

4.1 *Virtual POC circuit parameterization*

The Virtual POC circuit was synthesized from closed-form expression by prescribing the designated center frequency, f_n of 50 kHz. After the design methodology outlined in the preceding section, the values of L_n and C_n were subsequently calculated from expressions (17), (18) and (19), respectively. While fixing load resistance R_L was fixed and R_n was determined accordingly. Table 1 summarizes the Virtual PoC description and specifications.

Table 1. Design parameters of the passive BP-NGD Virtual PoC

Name	Parameter	Value
Center Frequency	f_n	50 kHz
Load Resistor	R_L	10 kΩ
Parallel Resistor	R_n	30 kΩ
Resonant Inductor	L_n	10 mH
Resonant Capacitor	C_n	1 nF

The numerical computation of the VTF and the corresponding frequency-domain GD and magnitude responses were conducted using MATLAB®, based on the analytically derived equations established in the previous section. The frequency-domain of the BP-NGD topology was subsequently validated through AC circuit simulation performed using the electronic circuit simulator NI MULTISIM®, to confirm the agreement between the analytically computed and simulated NGD responses within the defined passband. Figure 5 depicts the schematic design of passive PRLC circuit implemented using MULTISIM® circuit design software.

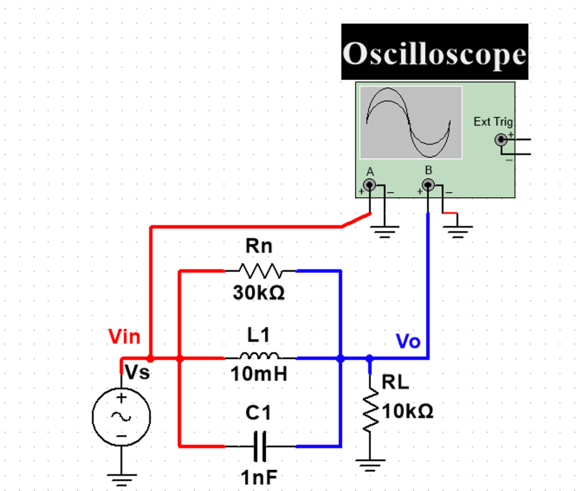

Figure 5. MULTISIM® schematic diagram of BP-NGD circuit as Virtual POC

The BP-NGD theoretical functionality was validated by simulation using MULTISIM® circuit design software. The next subsections are dedicated to a general description of the Virtual POC design and the simulated results validating the theoretical ones.

4.2 *Circuit simulation setup*

To theoretically analyze the proposed BP-NGD circuit, a comprehensive AC simulation was conducted using NI MULTISIM® software. The Virtual prototype BP-NGD circuit was characterized by using the AC sweep analysis, which provides the VTF response as a function of frequency. A linear frequency sweep configuration was applied in the AC simulation over the range of f_{min} = 10 kHz to f_{max} = 100 kHz with sufficiently dense frequency sampling to ensure adequate spectral granularity for accurate phase differentiation and subsequent GD extraction. The circuit schematic was constructed using the ideal passive components calculated based on the theoretical design equations derived in Subsection 3.2. To ensure that all reactive elements were operated in the linear region of the circuit, an AC signal source was established with amplitude of 1 V. A linear sweep configuration allows for the frequency sampling of all frequencies within the passband to occur at equal frequency intervals, which is essential for reliable numerical differentiation of the phase data. The three key parameters were extracted from the simulation data:

- Magnitude response $|H(j\omega)|$: to verify the BP-NGD circuit characteristic and confirm the expected insertion loss.
- Phase response $\phi(\omega)$: to examine nonlinear phase behavior essential for NGD realization.
- GD response $\tau_g(\omega)$: to compute via numerical differentiation of the simulated phase data to directly quantify the NGD at the center frequency.

A comparison of analytical predictions and simulated data across the transmission magnitude, phase and GD responses with the working frequency band were depicted in Figure 6a–c, respectively.

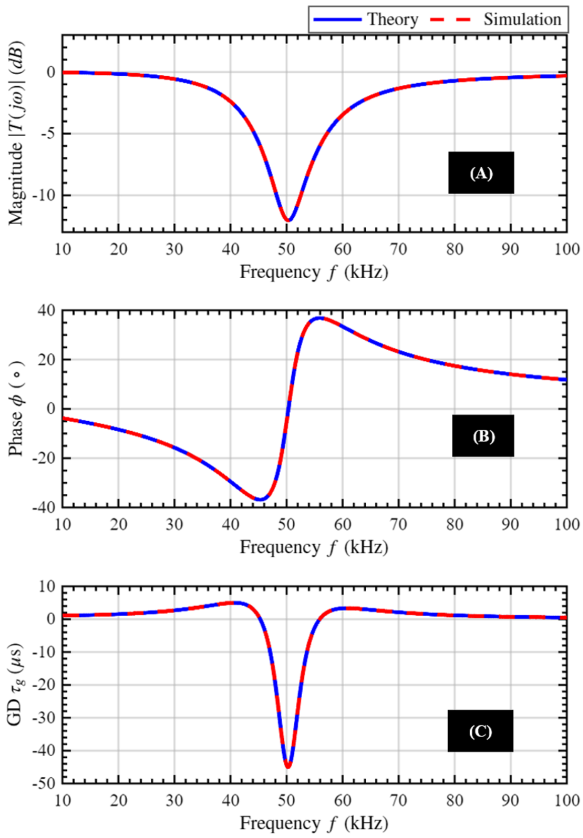

Figure 6. Comparison of theoretical and simulated responses of the proposed BP-NGD cell: VTF (a) magnitude, (b) phase and (c) GD

The results are in good agreement with the theory over the whole sweep range. The simulated GD has a sharp negative peak at the design center frequency, which is a signature of the BP-NGD behavior. The BP-NGD analysis results are summarized in Table 2.

Table 2. Theoretical versus simulated frequency-domain parameters of RLC BP-NGD cell

Name	Parameter	Theory	Simulation
Center Frequency	f_n (kHz)	50.32	50.28
Lower cut-off frequency	f_{c1} (kHz)	45.30	45.29
Upper cut-off frequency	f_{c2} (kHz)	55.91	55.90
Bandwidth	BW (kHz)	10.61	10.60
NGD Insertion loss	T_n (dB)	−12.04	−12.04
NGD Peak Value	GD_n (μs)	−45.02	−45.03

The above outlined frequency-domain analysis provides perceptions on the magnitude, phase, and GD responses characteristic of a passive parallel RLC BP-NGD circuit. However, this isolated frequency-domain analysis is insufficient to act as verification of the existence of the NGD phenomenon. In addition, it will not provide any immediate observation as to how a real-time variable signal will physically behave at the output of the circuit. Therefore, to support and demonstrate the fundamental time-advance aspect of the NGD phenomenon, time-domain analysis must be included in your work. The following section will review a time-domain analysis where input signals are both Gaussian-modulated and arbitrarily modulated waveforms. The resultant output signal anticipation behavior will be directly observed and confirmed; thus, the anticipated output signal of our proposed BP-NGD circuit will provide both a physically intuitive confirmation and a rigorous confirmation of the NGD response of the Virtual POC under study.

5. Time-domain analysis

This section extends the analysis of BP-NGD from AC sweep to transient response, allowing direct observation of input-output signal time-advance behavior as absolute proof of NGD phenomenon.

5.1 *Time-advance behavior*

The present analysis aims to verify the time-domain response of passive parallel RLC BP-NGD circuit through transient simulation conducted in NI MULTISIM®, satisfying the BP-NGD condition:

$$\tau_g(f_n) < 0. \tag{20}$$

To conceptually illustrate the expected time-advance behavior prior to simulation, Figure 7 presents an idealized representation of the input signal $x(t)$ and the corresponding BP-NGD circuit output signal $y(t)$.

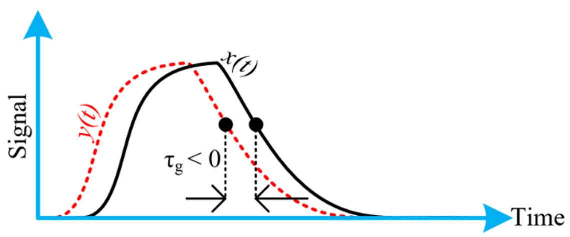

Figure 7. Ideal time-advance response of an arbitrary transient signal

It is clearly observed in Figure 7 the output envelope $y(t)$ depicted by the red dashed curve reaches its peak value before the input envelope $x(t)$ depicted by the solid black curve by a time interval equal to the magnitude of the NGD $|\tau_g| < 0$. The observed temporal precedence of the output modulated envelope relative to the input excitation is manifestation of the NGD phenomenon, wherein the GD assumes negative value at the designated frequency f_n, causing an output envelope to emerge ahead of the input envelope in time.

5.2 *Simulation response with gaussian waveform signal*

In this study, $V_{in,\,a}$ modulates a sinusoidal carrier at the NGD center frequency f_n, exhibits a Gaussian-modulated envelope with a rise time of approximately 236.9 µs and a fall time of approximately 240.8 µs, and a peak amplitude of $\max(V_{in,\,a}) \approx 49.9$ mV, as depicted in Figure 8a,b. A strong input-output correlation is observed where $\max(V_{out,a}) \approx 14.3$ mV, as shown in Figure 8b, yielding a peak amplitude ration of $\frac{\max(V_{out,a})}{\max(V_{in,a}) \approx -10.9}$ dB, in close agreement with the theoretically predicted NGD insertion loss of $T_n = -12$ dB established in the previous sections.

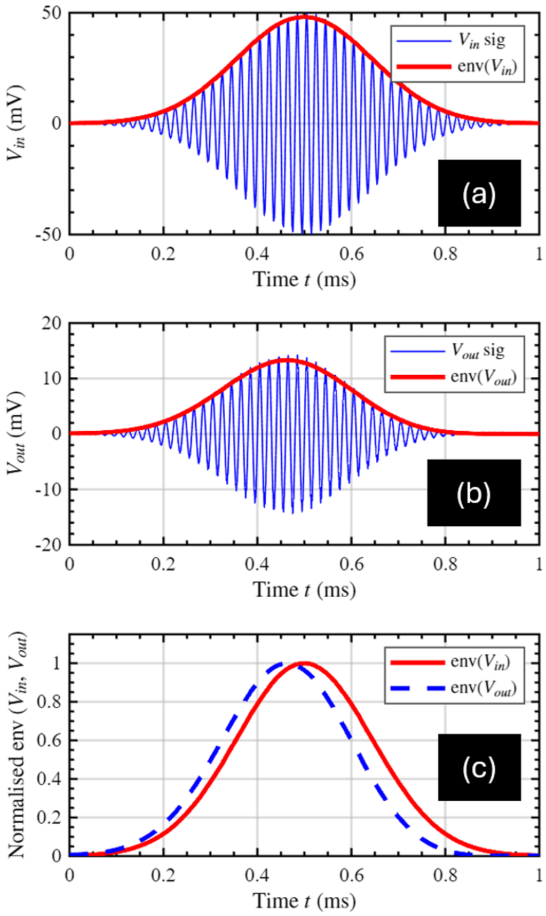

Figure 8. Time-domain analysis of BP-NGD Virtual PoC depicting plot of (a) v_{ina}, (b) v_{outa} and (c) env (v_{ina}) vs env (v_{outa}) in the range of [0, $t_{\max}$]

Despite the attenuation, the normalized envelope plots of Figure 8c, presenting the absolute values of the input and output envelopes $env(V_{in,a})$ (red solid curve) and $env(V_{out,a})$ (blue dashed curve) over $[0, t_{\max}]$ demonstrate a peak time-advance of approximately $\Delta t \approx -29.6$ µs < 0, wherein $t_{peak}(V_{out,a}) = 468.9$ µs clearly precedes $t_{peak}(V_{in,a}) = 498.5$ µs, confirming the unambiguous BP-NGD time-advance behavior. The discrepancy between $|\Delta t| = 29.6$ µs and the predicted $|\tau_{g,min}| = 45$ µs is physically expected. These results confirm the BP-NGD time-domain signature at $f = f_n$, with the output envelope exhibiting a clear and causally compliant time-advance.

5.3 *BP-NGD simulation response with arbitrary waveform signal*

In this study, $V_{in,b}$ modulates a sinusoidal carrier having frequency f_n = 50 kHz, exhibiting an arbitrarily modulated envelope with an asymmetric profile rise time of approximately 239.8 µs and fall time of approximately 633.1 µs and a peak amplitude of max $\left(V_{in,b}\right) \approx 999.38$ mV over [0, 1.4 ms], as depicted in Figure 9a,b, respectively.

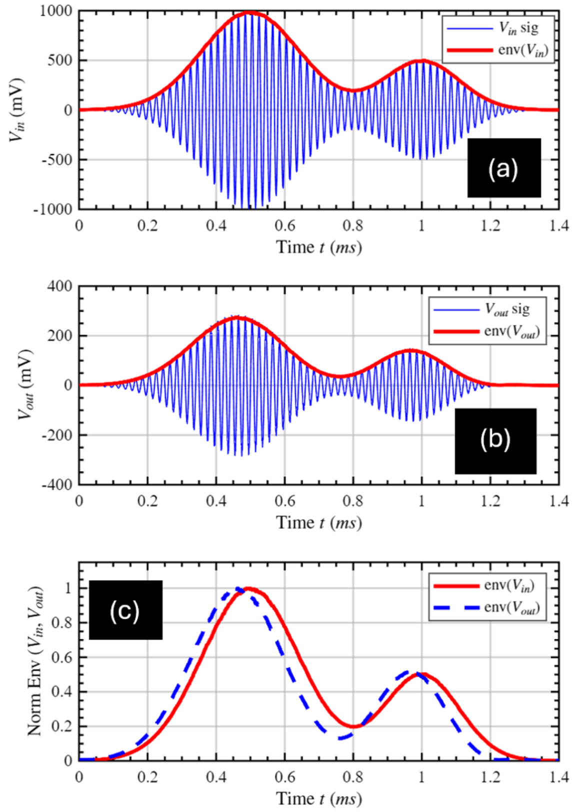

Figure 9. Time-domain analysis of BP-NGD Virtual PoC depicting plot of (a) $v_{in,b}$, (b) $v_{out,b}$ and (c) env($v_{in,b}$) vs env($v_{out,b}$) in the range of [0, $t_{\max}$]

A strong input-output correlation is observed, where $\max(V_{out,b}) \approx 284.1$ mV as shown in Figure 9c, yielding a peak amplitude ratio of $\max(V_{out,b})/max(V_{in,b}) \approx -10.93$ dB, consistent with the theoretically predicted NGD insertion loss of $T_n = -12.04$ dB. Despite the attenuation, the normalized envelope plots of Figure 9, presenting env$(V_{in,b})$ (red solid curve) and env$(V_{out,b})$ (blue dashed curve) over [0, t_{max}], demonstrate a peak time-advance of $\Delta t_b \approx -30.6$ µs < 0, wherein $t_{peak}(V_{out,b}) = 463$ µs clearly precedes $t_{peak}(V_{in,b}) = 493.6$ µs, confirming the unambiguous BP-NGD time-advance behavior. The consistency between $|\Delta t_b| = 30.6$ µs and the Gaussian result $|\Delta t_a| = 29.6$ µs demonstrates that the time-advance is a fundamental and generalizable property of the proposed network, independent of input signal morphology. The discrepancy with the predicted $|\tau_{g,min}| = 45$ µs is physically expected.

6. Conclusion

This study presents an analysis of a passive parallel RLC-type bandpass negative group delay (BP-NGD) network, specifically with respect to the time-domain response. The study provides the required theoretical support to calculate the

RLC circuit components directly from specifications. The prototype model was designed for a frequency of 50 kHz and measured approximately −45 μs of NGD, with an insertion loss of −12.04 dB, demonstrating strong agreement between theoretical predictions and NI Multisim® simulations. Crucially, transient analyses employing both Gaussian-modulated and arbitrarily modulated input waveforms unambiguously confirm the time-advance behavior of the output envelope without violating causality. The results validate that the observed time-domain advancement is a fundamental and signal-independent property of the proposed topology. The originality of this work lies in this comprehensive time-domain characterization, demonstrating that the time-advance behavior is a fundamental property rather than an artifact of specific input morphologies. Additionally, this study contributes on the closed-form analytical design methodology that enables the direct synthesis of RLC components from targeted NGD specifications, effectively bridging the gap between theoretical NGD phenomenology and practical low-frequency circuit implementation. These findings establish the effectiveness of passive RLC configurations for realizing NGD functionality in the low-frequency regime, with promising implications for signal synchronization and phase compensation applications. Future work will focus on integrating an operational amplifier to compensate for insertion loss and on extending the topology to multi-band BP-NGD configurations.

Conflict of interest

The authors declare no competing financial interest.

References

[1] B. Ravelo, A. Perennec, and M. Le Roy, "Synthesis of broadband negative group delay active circuits," In Proc. IEEE/MTT-S International Microwave Symposium, Honolulu, HI, USA, Jun. 3-8, 2007, pp. 2177-2180. https://doi.org/10.1109/MWSYM.2007.380357.

[2] J. Y. Cui, H. E. Silochi, R. Wieser, S. Junwen, H. Bilal, S. Ngoho, et al., "Familiarity analysis and time-advance experimental study of LP-NGD RC-circuit intended to operate with unity-normalized gain," *COMPEL - International Journal of Computational Mathematics in Electrical and Electronic Engineering*, vol. 43, no. 5, pp. 1007-1022, 2024. https://doi.org/10.1108/COMPEL-07-2023-0301.

[3] M. T. Abuelma'atti and Z. J. Khalifa, "A new CFOA-based negative group delay cascadable circuit," *Analog Integrated Circuits and Signal Processing*, vol. 95, no. 2, pp. 351-355, 2018. https://doi.org/10.1007/s10470-018-1172-y.

[4] A. Sommerfeld, *Lectures on Theoretical Physics: Optics*, vol. 4. Academic Press, 1964. [online]. Available: https://api.pageplace.de/preview/DT0400.9780323152396_A24400297/preview-9780323152396_A24400297.pdf. [Accessed Jun. 26, 2026].

[5] L. Brillouin, *Wave Propagation and Group Velocity*, vol. 8. Academic Press, 1960. [online]. Available: https://jontalle.web.engr.illinois.edu/Public/BOOKS/BrillouinWaveProgGroupVel.60.pdf. [Accessed Jun. 26, 2026].

[6] B. Segard and B. Macke, "Observation of negative velocity pulse propagation," *Physics Letters A*, vol. 109, no. 5, pp. 213-216, 1985. https://doi.org/10.1016/0375-9601(85)90305-6.

[7] M. W. Mitchell and R. Y. Chiao, "Negative group delay and 'fronts' in a causal system: an experiment with very low frequency bandpass amplifiers," *Physics Letters A*, vol. 230, no. 3-4, pp. 133-138, 1997. https://doi.org/10.1016/S0375-9601(97)00244-2.

[8] M. W. Mitchell and R. Y. Chiao, "Causality and negative group delays in a simple bandpass amplifier," *American Journal of Physics*, vol. 66, no. 1, pp. 14-19, 1998. https://doi.org/10.1119/1.18813.

[9] S. Chu and S. Wong, "Linear pulse propagation in an absorbing medium," *Physical Review Letters*, vol. 48, no. 11, p. 738, 1982. https://doi.org/10.1103/PhysRevLett.48.738.

[10] C. G. B. Garrett and D. E. McCumber, "Propagation of a Gaussian light pulse through an anomalous dispersion medium," *Physical Review A*, vol. 1, no. 2, p. 305, 1970. https://doi.org/10.1103/PhysRevA.1.305.

[11] H. Cao, A. Dogariu, and L. Wang, "Negative group delay and pulse compression in superluminal pulse propagation," *IEEE Journal of Selected Topics in Quantum Electronics*, vol. 9, no. 1, pp. 52-58, 2003. https://doi.org/10.1109/JSTQE.2002.807974.

[12] T. Nakanishi, K. Sugiyama, and M. Kitano, “Demonstration of negative group delays in a simple electronic circuit,” *American Journal of Physics*, vol. 70, no. 11, pp. 1117-1121, 2002. https://doi.org/10.1119/1.1503378.

[13] M. Kitano, T. Nakanishi, and K. Sugiyama, “Negative group delay and superluminal propagation: an electronic circuit approach,” *IEEE Journal of Selected Topics in Quantum Electronics*, vol. 9, no. 1, pp. 43-51, 2003. https://doi.org/10.1109/JSTQE.2002.807979.

[14] S. Lucyszyn and I. D. Robertson, “Analog reflection topology building blocks for adaptive microwave signal processing applications,” *IEEE Transactions on Microwave Theory and Techniques*, vol. 43, no. 3, pp. 601-611, 1995. https://doi.org/10.1109/22.372106.

[15] S. Lucyszyn, I. D. Robertson, and A. H. Aghvami, “Negative group delay synthesiser,” *Electronics Letters*, vol. 29, no. 9, pp. 798-800, 1993. https://doi.org/10.1049/el:1993053.

[16] G. V. Eleftheriades, A. K. Iyer, and P. C. Kremer, “Planar negative refractive index media using periodically L-C loaded transmission lines,” *IEEE Transactions on Microwave Theory and Techniques*, vol. 50, no. 12, pp. 2702-2712, 2002. https://doi.org/10.1109/TMTT.2002.805197.

[17] O. F. Siddiqui, M. Mojahedi, and G. V. Eleftheriades, “Periodically loaded transmission line with effective negative refractive index and negative group velocity,” *IEEE Transactions on Antennas and Propagation*, vol. 51, no. 10, pp. 2619-2625, 2003. https://doi.org/10.1109/TAP.2003.817556.

[18] C. D. Broomfield and J. K. A. Everard, “Broadband negative group delay networks for compensation of microwave oscillators and filters,” *Electronics Letters*, vol. 36, no. 23, pp. 1931-1933, 2000. https://doi.org/10.1049/el:20001377.

[19] C. Caloz and T. Itoh, “Application of the transmission line theory of left-handed (LH) materials to the realization of a microstrip ‘LH line’,” In Proc. IEEE Antennas and Propagation Society International Symposium, San Antonio, TX, USA, Jun. 16-21, 2002, pp. 412-415. https://doi.org/10.1109/APS.2002.1016111.

[20] J. Nako, C. Psychalinos, A. S. Elwakil, and B. J. Maundy, “Power-law negative group delay filters,” *Electronics*, vol. 13, no. 3, p. 522, 2024. https://doi.org/10.3390/electronics13030522.

[21] J. Nako, C. Psychalinos, B. J. Maundy, and A. S. Elwakil, “Elementary negative group delay filter functions,” *Circuits, Systems, and Signal Processing*, vol. 43, no. 6, pp. 3396-3409, 2024. https://doi.org/10.1007/s00034-024-02647-9.

[22] J. Nako, C. Psychalinos, A. S. Elwakil, and B. J. Maundy, “A note on the bandwidth of negative group delay filters,” *International Journal of Circuit Theory and Applications*, vol. 53, no. 1, pp. 477-484, 2025. https://doi.org/10.1002/cta.4132.

[23] B. Ravelo, “Similitude between the NGD function and filter gain behaviours,” *International Journal of Circuit Theory and Applications*, vol. 42, no. 10, pp. 1019-1035, 2014. https://doi.org/10.1002/cta.1902.

[24] B. Ravelo, “Unity direct chain with feedback series impedance based innovative negative group delay circuit,” *AEU - International Journal of Electronics and Communications*, vol. 91, pp. 11-17, 2018. https://doi.org/10.1016/j.aeue.2018.04.018.

[25] M. Guerin, F. Wan, K. Gorshkov, X. Huang, B. Tishchuk, F. E. Sahoa, et al., “High-pass NGD characterization of resistive-inductive network based low-frequency circuit,” *COMPEL - The International Journal for Computation and Mathematics in Electrical and Electronic Engineering*, vol. 40, no. 5, pp. 1032-1049, 2021. https://doi.org/10.1108/COMPEL-05-2021-0160.

[26] Y. Zhang, X. Su, R. Wieser, R. Sanchez Galan, and B. Ravelo, “Reshaping of distorted signal with low-pass type negative group delay RL-network circuit,” *Circuits, Systems, and Signal Processing*, vol. 44, no. 4, pp. 2308-2329, 2025. https://doi.org/10.1007/s00034-024-02953-2.

[27] S. Junwen, C. Junyan, H. E. Silochi, R. Wieser, R. S. Galan, N. M. Murad, et al., “Positive-to-negative tunable delay circuit designed with NGD RC network,” *International Journal of Circuit Theory and Applications*, vol. 52, no. 10, pp. 5010-5024, 2024. https://doi.org/10.1002/cta.4010.

[28] B. Ravelo, F. Wan, J. Nebhen, W. Rahajandraibe, and S. Lalléchère, “Resonance effect reduction with bandpass negative group delay fully passive function,” *IEEE Transactions on Circuits and Systems II: Express Briefs*, vol. 68, no. 7, pp. 2364-2368, 2021. https://doi.org/10.1109/TCSII.2021.3059813.

[29] A. Zhang, J. Xu, and Z. Liu, “A microstrip linear-phase BPF using dual-band negative group delay equalizers,” *IEEE Microwave and Wireless Technology Letters*, vol. 34, no. 4, pp. 387-390, 2024. https://doi.org/10.1109/LMWT.2024.3361896.

[30] H. Du, R. Yang, T. Gu, X. Zhou, S. Yazdani, E. Sambatra, et al., “Analysis, design and experimentation of high-pass negative group delay lumped circuit,” *Circuit World*, vol. 49, no. 2, pp. 180-191, 2023. https://doi.org/10.1108/CW-07-2020-0131.

[31] C. Yujie, L. Jianing, S. Moussa, R. Wieser, R. S. Galan, M. Guerin, et al., “Feasibility study of multistage low-pass NGD circuit design methodology using RL-network,” *International Journal of Circuit Theory and Applications*, vol. 54, no. 1, pp. 132-141, 2026. https://doi.org/10.1002/cta.70033.

[32] E. J. R. Sambatra, Y. C. Mombo Boussougou, L. Ramifidisoa, J.-P. Kouadio, S. Ngoho, A. Jaomiary, et al., “Band pass negative group delay demonstration on a VHF RLC parallel passive lumped circuit,” *Advances in Electromagnetics*, vol. 11, no. 1, pp. 9-21, 2022. https://doi.org/10.7716/aem.v11i1.1858.

[33] E. J. R. Sambatra, S. Ngoho, F. Haddad, M. Guerin, G. Fontgalland, W. Rahajandraibe, et al., “Electrothermal analyses of bandpass NGD RLC-network topologies,” *Advances in Electromagnetics*, vol. 12, no. 1, pp. 77-86, 2023. https://doi.org/10.7716/aem.v12i1.2125.

[34] R. Randriatsiferana, Y. Gan, F. Wan, W. Rahajandraibe, R. Vauché, N. M. Murad, et al., “Study and experimentation of a 6-dB attenuation low-pass NGD circuit,” *Analog Integrated Circuits and Signal Processing*, vol. 110, no. 1, pp. 105-114, 2022. https://doi.org/10.1007/s10470-021-01826-x.

[35] T. Shao, Z. Wang, S. Fang, H. Liu, and Z. N. Chen, “A full-passband linear-phase band-pass filter equalized with negative group delay circuits,” *IEEE Access*, vol. 8, pp. 43336-43343, 2020. https://doi.org/10.1109/ACCESS.2020.2977100.

[36] M. Guerin, Y. Liu, A. Douyère, G. Chan, F. Wan, S. Lalléchère, et al., “Design and synthesis of inductorless passive cell operating as stop-band negative group delay function,” *IEEE Access*, vol. 9, pp. 100141-100153, 2021. https://doi.org/10.1109/ACCESS.2021.3095814.

[37] R. Vauche, R. A. B. Mefteh, F. Haddad, J. Nebhen, W. Rahajandraibe, F. Wan, et al., “Experimental time-domain study for bandpass negative group delay analysis with Lill-shape microstrip circuit,” *IEEE Access*, vol. 9, pp. 24155-24167, 2021. https://doi.org/10.1109/ACCESS.2021.3056221.